Sensor and Simulation Notes

Note 575

21 February 2016

Design of an Ultra-Wideband Ground-Penetrating Radar System Using Impulse Radiating Antennas

J.B. Rhebergen and A.P.M. Zwamborn
TNO Physics and Electronics Laboratory, The Netherlands.

and

D. V. Giri

Dept. of ECE, University of New Mexico, Albuquerque, NM, USA

Pro-Tech, 11-C Orchard Court, Alamo, CA 94507, USA

Abstract

At TNO-FEL in The Hague, Netherlands, one of the research programs is to explore the use of ultra-wideband (UWB) electromagnetic fields in a bi-static ground-penetrating radar (GPR) system for the detection, location and identification of buried items of unexploded ordnance (e.g. land mines). In the present paper we describe the current status of the development of this system. The UWB ground-penetrating radar system is designed to operate in the frequency band from 200 MHz to 3 GHz and uses impulse radiating antennas (IRAs) as transponders to radiate and receive very short electromagnetic pulses from a short distance above the soil. The receiving IRA is similar to the transmitting IRA and is connected to a receiving unit which comprises of an attenuator; time gate switch, trigger delay generator and a sampling oscilloscope. A personal computer is used to control the equipment. In order to perform controlled radar experiments, a full-size experimenting and testing facility has been erected on the premises of TNO- FEL. This note describes the GPR facility and all associated equipment.

1. System Design

To design an UWB GPR system (see Figure 1) for detection, location and identification of land-mines the following points have to be successfully combined.

- generation of UWB EM field (i.e. source)
- radiation of UWB EM field (i.e. antenna)
- characterization of the soil and air/earth interface
- reception and synthesis of scattered fields
- signal processing techniques and identification of objects
- controlled experimental test environment

This paper concentrates mainly on the system design. The signal processing aspects are, for the time being, saved for a future follow-up paper although some preliminary work has taken place [1]. An overview of the overall system concept is shown in Figure 1. The target volume is illuminated by an ultra-wideband electromagnetic field, with an angle of incidence chosen to maximize energy transmission into the ground, whilst minimizing reflection from the ground/air interface. Presently, the main interest is in objects varying in size from about 5 cm up to about 75 cm. In air this corresponds to wavelengths of 1.5 m to 0.1 m. Consequently the frequency range of interest extends from 200 MHz up to 3 GHz.

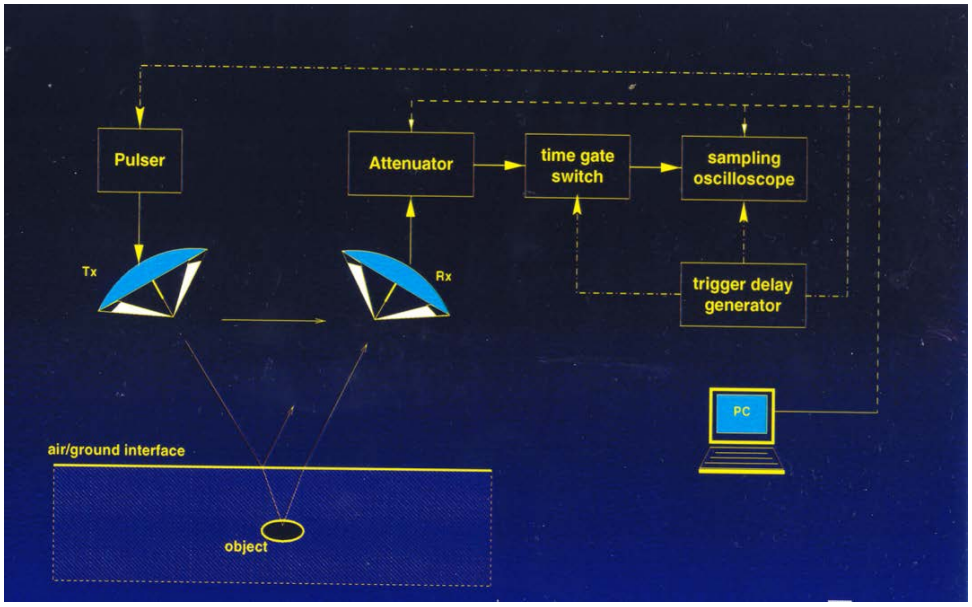

Figure 1. Schematic block diagram of a generic UWB GPR system

The principal goal is to perform the needed analytical and design work to support the construction of an experimental test facility, where targets can be buried in a sand medium and illuminated by an ultra-wideband electromagnetic field. The scattered fields have to be observed and diagnosed for the purpose of building an electronic database containing the responses of a large number of buried objects.

2. Generation of UWB EM Fields

For our UWB GPR system, it was decided to use a solid state pulse generator with an approximate double exponential voltage waveform. Such a waveform can be modeled by

$$V(t) = V_o\,[\,e^{-\beta(t-t_o)} - e^{-\alpha(t-t_o)}\,]\,u(t-t_o)\ \ V$$

V_o = field intensity constant V

α = decay constant rad/s (1)

β = risetime constant $(\alpha >> \beta)$ rad/s

$u(t-t_o)$ = unit step function

t_o = time shift s

In our case, the parameters are

$$V_o = 9.635kV \tag{2}$$

$$\alpha = 2.\,x\,10^{10}\ s^{-1} \quad and \quad \beta = 2.5\,x\,10^{8}\ s^{-1} \tag{3}$$

This gives rise to a Fourier spectrum

$$\tilde{V}(\omega) = V_o\left(\frac{1}{j\omega + \beta} - \frac{1}{j\omega + \alpha}\right)$$

$\tilde{V}(\omega)$ = *Fourier transform of* $V(t)$ $\frac{V}{Hz}$

$\omega = 2\pi f$ = *radian frequency* *radians / s*

$j = \sqrt{-1}$ (4)

Since the magnitude of the far field is proportional to the derivative of the voltage waveform, a better radiated spectrum (enhanced bandwidth) is obtained when compared to sinusoidal mono-cycles. The pulser is designed to drive a 50 Ohm load, is fully protected against open and short circuit loads and has a pulse repetition frequency of 1 kHz. The pulse has a 10% to 90% rise time of about 100 ps and a full-width half-maximum (FWHM) time of 3 ns.

3. Radiation of UWB EM fields

Many commercially available wideband antennas have poor performance when it comes to radiating very short pulses. Part of the UWB GPR system design entailed the design of an IRA for ground penetrating radar applications. The upper frequency limit f_{upper} of such and antenna is determined by the pulse rise time t_{rise} while the lower frequency limit f_{lower} is determined by the dimensions of the reflecting dish. Experiments have shown [15] that an antenna with a 4 m reflecting dish and a $\pm$ 60 kV switch with a 85 ps rise time has a bandwidth extending from 50 MHz to 4 GHz with a field strength of 4 kV/m at 300m. The frequency range of interest in our case is from about 200 MHz to 3 GHz. Hence the diameter of the reflecting dish was proposed to be in the order of 1 m.

4. Soil Characterization

Electromagnetic waves are damped considerably when traveling through a medium with conductivity greater than zero. In our experimental set-up the angle of incidence and incident polarization are chosen such as to maximize the energy transfer from the transmitter into the ground. This is based on the technique of pulse matching into the ground developed in [10], for vertical polarization. If frequencies are much larger than the relaxation frequency of the ground ($f_{relax} = \sigma / \varepsilon$) , there is an angle of incidence at which there is very little reflection of the incident wave from the air/ground interface.

This is called the high-frequency Brewster angle. For $f >> f_{relax}$ it can be shown that reflection is minimal (theoretically zero) when,

$$\tan(\psi_B) = \sqrt{\varepsilon_r} \qquad (5)$$

When σ = 0.01 S/m and ε_r = 10, then the relaxation frequency of the ground f_{relax} = 113 MHz. Hence when the conductivity $\sigma \leq$ 0.01 S/m, which is quite typical, the radiated spectrum of the IRA will be transmitted into the ground with minimum reflection. Table 1 shows some examples of high-frequency Brewster angles at various values of permittivity.

Table 1. Brewster angle as a function of soil permittivity

ε_r	2	4	6	8	10
ψ_B	54.73^o	63.42^o	67.79^o	70.53^o	$72.4^o 5$

5. Reception and synthesis of scattered fields

The receiving system consists of:

- Receiving antenna, similar to transmitting antenna
- Processing unit (data acquisition).

The processing unit has to perform two tasks:

- Recording and preprocessing the incoming signal, reducing noise, clutter and distortion caused by the signal path;
- Performing some signal processing on the scattered field in order to be able to identify the buried objects.

Data acquisition and processing is done by a sampling (digitizing) oscilloscope able to perform measurements on signals with bandwidth of up to 20 GHz. The input signal cannot be measured reliably at just one instance, which is why a sampling oscilloscope employs a repetitive sampling architecture. This in turn requires the transmitted pulse to be repetitive as well. Arithmetic averaging of the repetitive input signal can significantly reduce the noise (and jitter) on the received scattered field signal. Gating allows isolation of the part of the signal due to the buried objects.

6. Signal processing and identification

Until 1980, almost all of the work in the field of ground penetrating radar was directed towards the detection of buried objects. Only very few attempted the problem of target identification (or classification), which is a problem far more severe than the identification of aerospace targets by conventional radars where the target can literally be seen and the class of false targets is limited in scope. Underground there are varieties of undesired targets that complicate the task. Furthermore, the ground medium involved, is usually lossy, inhomogeneous and electrically weather-dependent. This problem, together with the presence of the air-ground interface, makes the task of subsurface target identification truly formidable. It was suggested by some authors [3, 4] that the singularity expansion method (SEM) is one of the few methods capable of performing identification of objects [2]. This method is based on the theoretical observation that all objects have natural resonant frequencies that depend on their size, shape and the material decomposition only and not on the orientation of the object or on the direction of the incoming field. When a target is hit by a short electromagnetic pulse, the target will “ring” and radiate a scattered field that contains as prominent constituents a set of damped sinusoids. These sinusoids represent the natural resonant frequencies. The bandwidth of the ultra-wideband system must be large enough to cover all the resonant frequencies of interest. The SEM will be exploited in the current problem of classification of the buried object for the calculation of the internal resonances of the buried object by processing the reflections or backscattering from the objects. Some initial analysis with synthetic data has already been performed [1].

7. Design and Construction of an IRA

The paraboloidal reflector antenna fed by a pyramidal horn has found wide-spread application in radar and communication engineering. The reflector antenna also has very useful characteristics when it is fed by two or four conductor transmission lines. A dispersion-less wideband antenna with a nearly flat radiating spectrum is desirable for short pulse applications. The reflector IRA employs a paraboloidal reflector fed by TEM lines [5-9], and is an example of an aperture antenna. It is well known that the radiated field from an aperture antenna consists of a spatial integration of the aperture fields over the aperture, while the temporal behavior of the aperture field is differentiated in the far field. In a practical situation, the illuminating field or the aperture field is a double exponential waveform and the radiated field then becomes impulse-like with a very large bandwidth ratio. The reflector IRA under consideration consists of a paraboloidal reflector fed by two pairs of coplanar feed plates as illustrated in Figure 2.

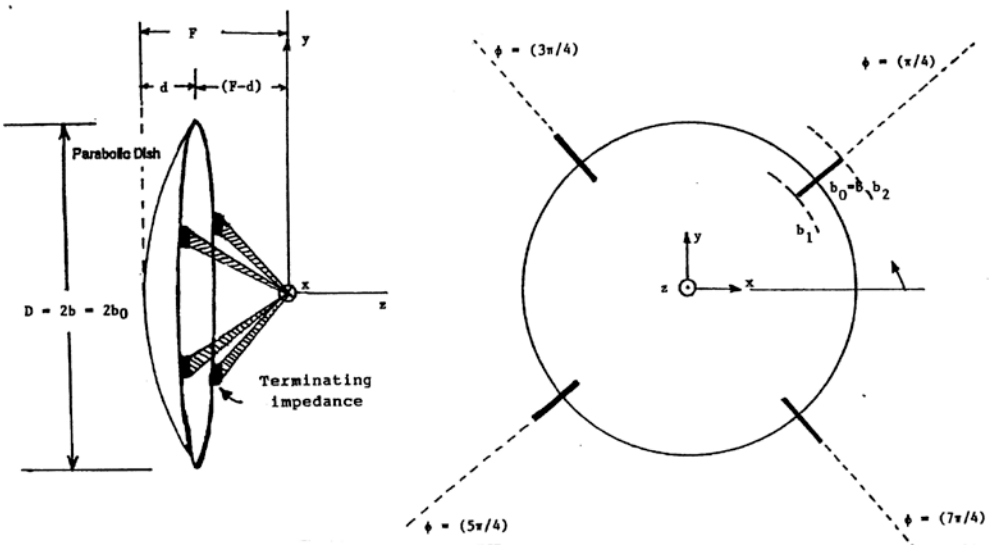

Figure 2. An illustration of a reflector fed by a pair of coplanar conical TEM lines.

Coplanar feed plates are chosen over the more conventional facing plate geometry to minimize the aperture blockage effects. To reduce the aperture blockage, the feed plates are required to be narrow, resulting in feed impedances of several hundreds of Ohms. The 400 Ohm lines are connected in parallel resulting in a net feed impedance of 200 Ohm. The aperture area should be as large as practically possible, since the far field is proportional to the square root of this area for a constant voltage at the feed. The magnitude of the far field is proportional to the aperture

area for a constant aperture field. The pulse generator has to be of the differential type to avoid common mode currents on the feed plates, which could distort the desired features in the far field. Since E_{far} is proportional to (dV/dt) , it is desirable to maximize this rate of rise of the incident field or the voltage pulse.

Two identical reflectors were manufactured with the following characteristics.

- One piece, spun aluminum, paraboloidal surface
- Diameter D = 900 mm
- Focal length F = 337.5 mm
- Profile accuracy < 1.5 mm
- $f_d = F/D = 0.375$

The desired rise time of 100 ps implies an upper 3 dB frequency of 3.5 GHz which gives rise to wavelengths in air of 85.7 mm. The surface tolerance of the reflector is small compared to the shortest wavelength and hence it is acceptable.

Next, we look at an estimation of boresight waveforms. For analysis purposes, one could consider a single (two conductor) coplanar feed, although in practice we used two such feed lines connected in parallel for a more uniform illumination of the reflector (see Figure 2). When the reflector IRA was originally proposed [5], the boresight radiation was predicted to consist of a feed step followed by an impulse-like behavior. It was also shown that the total area under these two parts of the radiated waveform (i.e. prepulse plus impulse) is zero. This means, that there is no DC component in the radiated waveform consisting of the prepulse and the impulse. This further implies that the portion of the radiated waveform after the impulse must have a net zero area in itself. The post impulse portion consists of diffracted signals from the feed plate and the circular rim of the paraboloidal reflector. Analysis [6] has extended this result by chronologically considering the various temporal elements of the boresight radiation, which is illustrated in Figure 3. Let us assume that the voltage pulse generator is switched on at t = 0, and the observer is at a distance r (= z) to the right of the focal point of the paraboloid. These temporal elements as depicted in Figure 3 are:

- *Prepulse* $E_{y1}(r, t)$
- *Main pulse of interest* – impulse $E_{y2}(r, t)$
- *Postpulse*
    a) feed plate diffraction consisting of two parts
        - plate edge on plate of finite width, large compared to wavelength
        - plate of finite width, small compared to wavelength, modeled by circular cylinder
    b) edge diffraction from the circular rim of the parabolic reflector

- Entire Pulse constraints: low-frequency dipole moment radiation and no radiation at zero frequency,

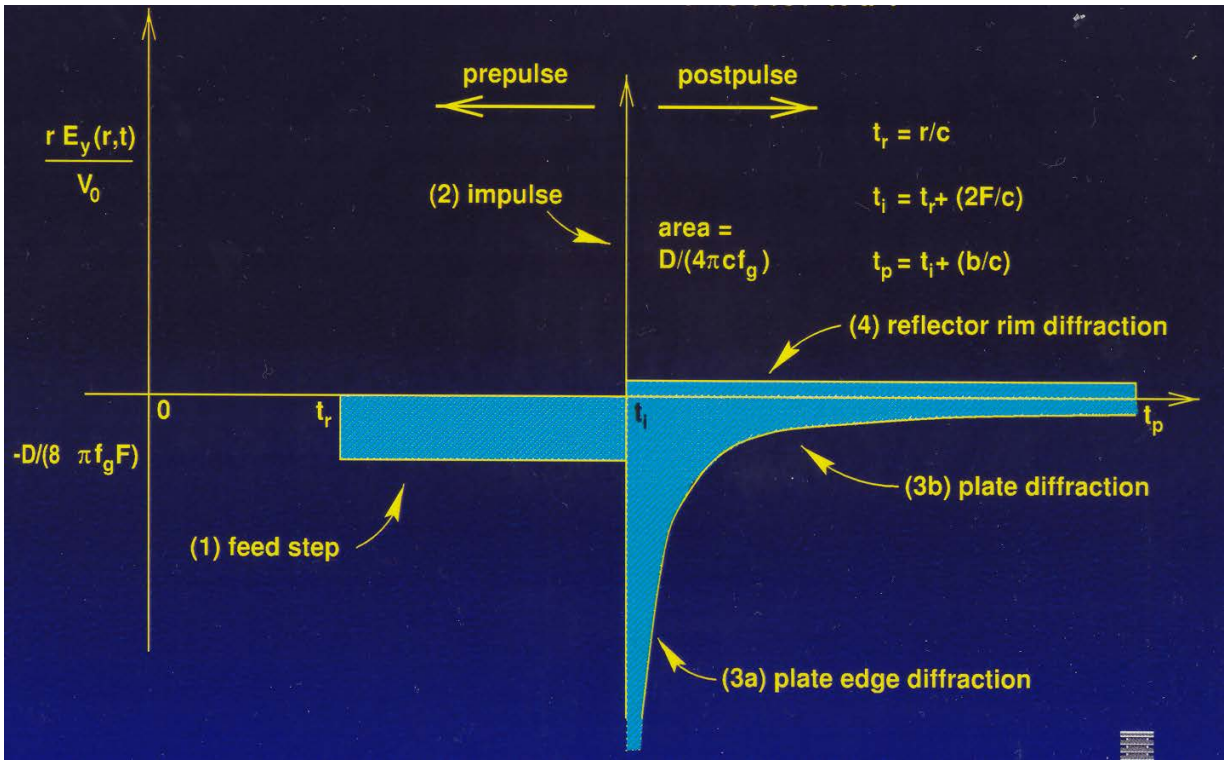

Figure 3. On-axis radiation form canonical reflector IRA fed by a step function source

The far field $\vec{E}_f(\vec{r},t)$ is given by

$$\vec{E}_f(\vec{r},t) = \vec{1}_y \; E_y(r,t), \quad \text{where} \tag{6}$$

$$E_y(r,t) = \sum_1^4 E_{yi}(r,t) \tag{7}$$

+low-frequency radiation from dipole moments resulting in time integral constraints on entire pulse

Detailed, closed-form expressions for the components $E_{yl}(r,t)$ in the above expression, are available in [7]. The results of equation (6) are illustrated in Figure 3. The time-integral constraints imposed by the low-frequency radiation are,

i) the complete first-time integral of the radiated waveform must be zero, and

ii) the second-time integral must be proportional to the late-time dipole moments.

8. Feed plates, termination and matching

The feed plates form a parallel combination of 2 x 400 Ohm conical TEM lines, giving the IRA an input impedance of 200 Ohms [11-13]. Matching to the 50 Ohm pulse source is done by means of balun. Suitable high-frequency, high-voltage, and high-impedance cables are difficult to find. Finally a 100 Ohm flexible cable with a PTFE dielectric was chosen. The latter is bound to introduce some dispersion. Termination of each feed plate at the dish edge consists of a net DC impedance of 200 Ohms. The insulating spacer is a high density polyethylene slab the dimensions of which are optimized experimentally. Capacitance of the slab is trimmed by drilling holes (tuned with help of TDR measurements at the antenna terminal. The Terminating resistor network, consist of a series-parallel network (5 by 5) of 1 W, 200 Ohm carbon composite resistors of 10% tolerance. Thus total heat dissipation is not a problem. Since the length of the resistor chain is > 10 cm, the voltage stand-off (of the order of 10 kV/cm) is not seen to be a problem either.

9. Far field of the IRA

If an aperture antenna of diameter D is illuminated by a CW field of frequency f, then the far field is determined by the distance r such that,

$$r \geq \frac{2D^2}{\lambda} \qquad (8)$$

which is obtained by requiring that $\Delta_r \leq (\lambda/16)$ where Δ_r, is the path difference of the edge ray and the central ray from aperture to observer. For pulsed antennas one can define a clear time $t_c = (\Delta_r / c)$ and require that $t_c < t_{rise}$ of the incident pulse. It is seen that

$$t_c = \frac{1}{c}\left[\sqrt{\frac{D^2}{4}+r^2} - r\right] \qquad (9)$$

Requiring that $t_c < t_{rise,}$ it is observed from Table 2 that the observation point has to be greater than 8 m, to be in the far field, by a comparison of the clear time with the rise time of 100 ps. The radiated fields on the bore-sight are known in closed form in the far field [5 to 9]. Russian researchers [14] have worked out near and far field expressions of the E-field on the boresight of an IRA. Using these expressions, we have estimated the on-axis E-field at various distances in the near field and far field of the antenna. This is the subject of the next subsection. Although 8 m is the minimum distance to be in the far field, the actual experiments of illuminating targets can be performed at shorter distances in the nearfield.

TABLE 2 - Clear time *t*, for a reflector diameter *D* = 0.9 m

r (m)	$r + \Delta_r \ (m)$	Δ_r (mm)	$t_c = \Delta_r / c \ (ps)$
1.0	**1.096**	**96**	**320.0**
2.0	**2.050**	**50**	**166.6**
2.5	**2.540**	**40**	**133.3**
3.0	**3.033**	**33**	**110.0**
3.5	**3.529**	**29**	**96.6**
4.0	**4.025**	**25**	**83.3**
5.0	**5.020**	**20**	**66.6**
8.0	**8.012**	**`2**	**40.0**
10.0	**10.010**	**10**	**33.3**

The near and far field characteristics are given in Table 3.

Table 3. Near and far field characteristics of the IRA on bore sight axis

Quantity	Near field	Far field
Distance r	5m	10m
Clear time	66 ps	33.3 ps
Prepulse amplitude	-255 V/m	-127 V/m
Prepulse duration	2.25 ns	2.25 ns
Impulse peak	5.9 kV/m	3.8 kV/m
Impulse duration	85 ps	60 ps

The pulse is broader and has more low-frequency components in the near field. In fact, very near the antenna, for example at the feed point, the electric field is similar to the voltage pulse which is a double exponential waveform. The differentiation occurs in the far field and the transformation from near to far field is gradual and not abrupt. This transformation can be experimentally observed by measuring the electromagnetic field on-axis, as one moves away from the focal region. These values have been experimentally verified during initial measurements and compare favorably with the above table. Expressions for the radiated

spectrum are available in literature as mentioned earlier. Calculations for our IRA results in the values listed in Table 4.

Table 4. Calculated bore-sight values for a distance of r = 10m

Quantity	Value
Peak E -field	2.85 kV/m +/- 12%
f_{low} (3 dB)	80 MHz
f_{high} (3 dB)	10 GHz
Band ratio	125
Band ratio decades	2.0976

Measurements indicate that the actual performance is not quite as good as theoretically predicted.

10. UWB GPR Experimental Facility

To be able to test the newly developed UWB GPR system and to perform experiments in a controlled environment, a full scale experimental test facility was erected on the premises of TNO-FEL. This facility has been developed in cooperation with the Delft University of Technology and will be used to illuminate objects buried in a realistic sand medium with an ultra-wideband electromagnetic field. The electromagnetic field scattered by the buried object has to be recorded and diagnosed for the benefit of developing a computer database containing the responses of a large number of potential targets (i.e. land-mines etc.). The sand box formation is shown in Figure 4.

Figure 4. Sand box under construction

The sand box construction is preferred because; different types of soil can be filled in the box. The experimental facility consists of a buried wooden box. The dimensions of this box are 10 m x 10 m wide and 3 m deep. Special care has been taken not to use any metal parts in the construction of the box or in the vicinity thereof. The sand-box is filled with clean homogeneous river sand. In order to keep the condition of the sand in the box optimal and to prevent pollution from the outside (for example ground water) entering the box, a drainage system was installed and the inside of the box was covered with a watertight plastic lining. To prevent the weather from influencing the test conditions and to protect the measuring equipment, a large tent covers the entire site. While filling the box with sand, special care was taken to get a homogeneous profile. Initial tests indicated that this was not entirely successful but should be good enough to work with. Later on we might choose to empty the box and refill it with a ground (soil) of a different composition. To facilitate the measurement of EM transmissions into the ground a square PVC tube running from the surface of one side to the bottom of the other side has been installed about one meter from the edge of the sand-box.

Example test objects are shown in Figure 5.

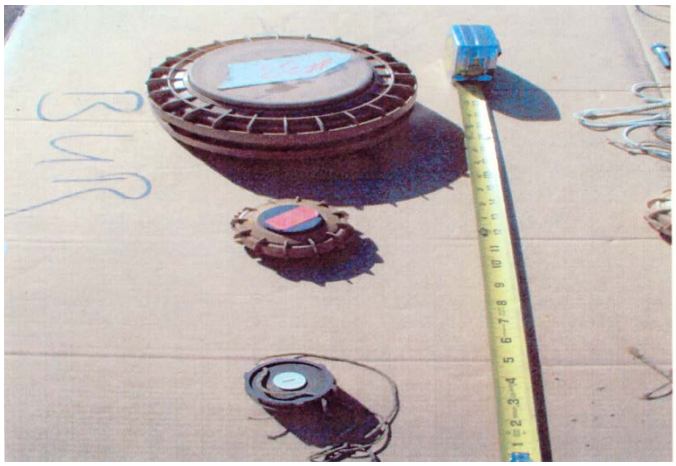

Figure 5. Examples of test objects buried in the sand

The top most test object in Figure 5 is an anti-tank mine which is relatively easy to detect because of the large metallic content. However, the anti-personnel mines shown in Figure 5 are harder to find. The arrangement of the transmitting and receiving IRA designed to illuminate the objet at Brewster angle is shown in Figure 6.

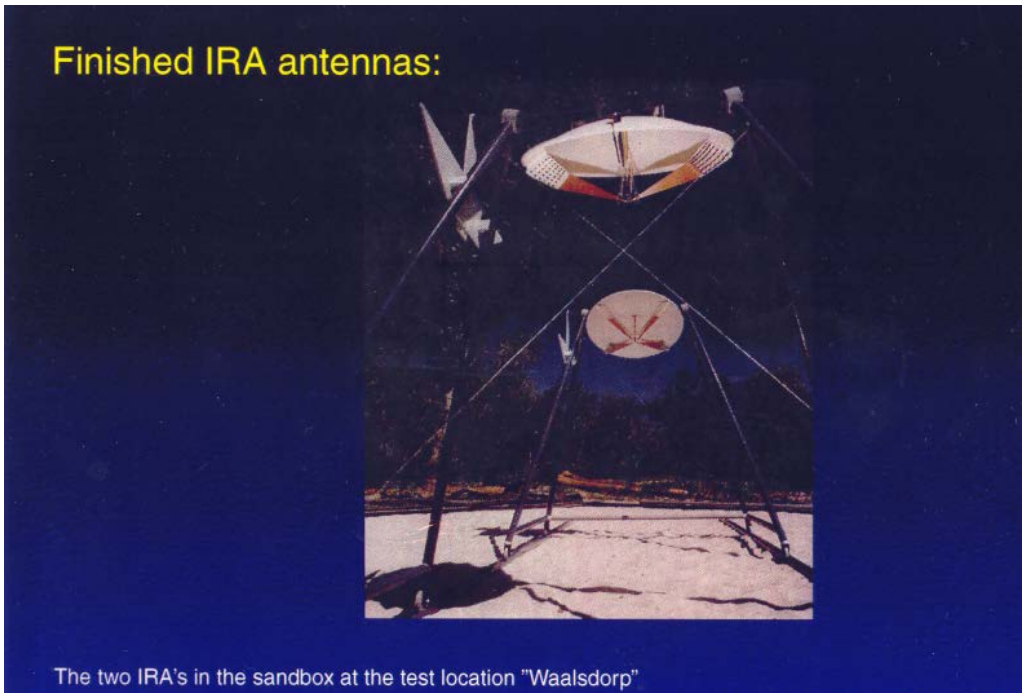

Figure 6. The completed transmitting and receiving IRAs on A-frames at the UWB GPR facility

We do not see the sand box in Figure 6 since it is buried under the ground, with the top of the sand box at the ground level. A typical measurement is shown in Figure 7.

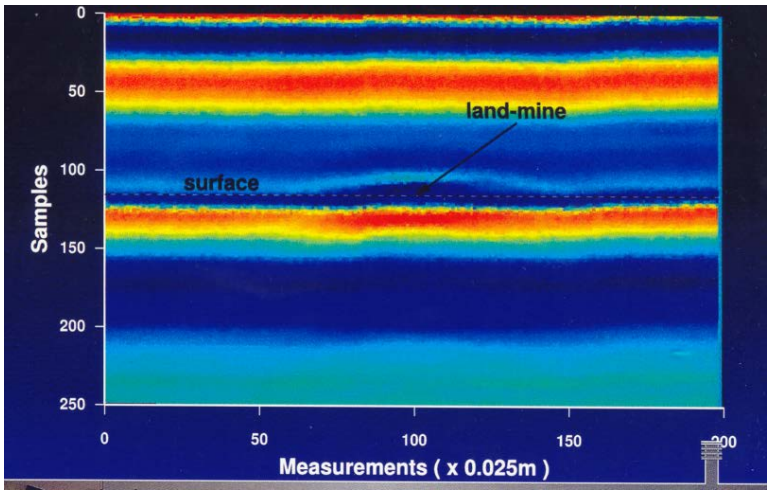

Figure 7. Typical measurement

11. Summary

This note is about describing the UWB GPR measurement facility. The design of the facility permits filling the underground sand box with different types of soils, as needed. It also permits burying known test objects and getting their scattered fields. The scattered field data can then be processed to get the Singularity Expansion Method (SEM) parameters of the test object such as complex natural frequencies. With this knowledge, one can construct a data base of known land mines and their specific signatures.

REFERENCES

[l] J. LoVetri, S. Primak, B.J.A.M. van Leersum and A.P.M. Zwamborn, "Feasibility study into the identification of land-mines using UWR radar and analysis using synthesized data", presented at EUROEM'98, Tel Aviv, to be published in "Ultra-Wideband Short-Pulse Electromagnetics 4" June 1998.

[2] C.E. Baum, E.J. Rothwell, K.M. Chen and D.P. Nyquist, "The Singularity Expansion Method and its application to target identification", Proc. of the IEEE, vol. 79, no. 10, 1991, pp. 1481-1492

[3] C.E. Baum, '"Signature-based target identification and pattern recognition", IEEE Antennas and Propagation Magazine, vol. 36, no. 3, pp. 44-51, 1994.

[4] C.E. Baum, L. Carin and A.P. Stone, "Ultra-wideband Short-pulse Electromagnetics 2", Plenum Press, New York, ISBN 0-306-45502-X, 1996.

[5] D.V. Giri and C.E Baum, "Temporal and spectral radiation on bore-sight if a reflector type of impulse radiating antenna ([RA)", published in [4].

[6] D.V. Giri and C.E. Baum, "Radiation of impulse-like transient fields", Sensor and Simulation Note 321, November 1989.

[7] D.V. Giri and C.E. Baum, "Reflector IRA design and bore-sight temporal waveforms", Sensor and Simulation Note 365, February 1994.

[8] D.V. Giri, H. Lackner, I.D. Smith, D.W. Morton, C.E. Baum, J.R. Marek, D. Scholfield and W.D. Prather, "A reflector antenna for radiating impulse-like waveforms", Sensor and Simulation Note 382, July 1995.

[9] D.V. Giri, "Radiated spectra of impulse radiating antennas (IRAs)", Sensor and Simulation Notes 386, November 1995.

[10] C.E. Baum, "The Brewster Angle Wave Matcher", Sensor and Simulation Notes 37, March 1967.

[11] C. E. Baum, D.V. Giri and R.D. Gonzalez, “Electromagnetic field distribution of the TEM mode in a symmetrical two-parallel plate transmission line”, Sensor and Simulation Note 219, April 1976.

[12] F.C. Yang and L. Marin, “Field distribution on a two-conical plate and a curved cylindrical plate line”, Sensor and Simulation Note 229, September 1977.

[13] J.J.A. Klaasen, “An efficient method for the performance analysis of bounded-wave nuclear EMP simulators”, Sensor and Simulation Note 345, August 1992.

[14] O.V. Mikheev, S.A. Podosenov, K. Yu. Sakharov, A.A. Sokolov, Y.G. Svekis and V.A. Turkin, “New method for calculating pulse radiation from an antenna with a reflector”, IEEE Transactions on Electromagnetic Compatibility, Volume 39, No. 1, pp 48-54, February 2007.

[15] D. V. Giri, ***High-Power Electromagnetic Radiators: Nonlethal Weapons and Other Applications***, Published by Harvard University Press, 2004, Section 5.3, pp 96-109.